ACS APPLIED ENERGY MATERIALS

Open Access
This article is licensed under CC-BY-NC-ND 4.0

www.acsaem.org
Article

Unveiling Electrolyte Design Principles for Sodium-Ion Batteries Using Combinatorial Electrochemistry and Machine Learning-Assisted Analysis

Published as part of ACS Applied Energy Materials special issue "Material and Interface Design in Next-Generation Batteries".

Manai Ono, Misato Takahashi, Ryo Tamura,* and Shoichi Matsuda*

Cite This: ACS Appl. Energy Mater. 2026, 9, 1405−1411

Read Online

ACCESS | Metrics & More | Article Recommendations | Supporting Information

ABSTRACT: To accelerate the development of high-performance electrolytes for sodium-ion batteries (SIBs), we systematically investigated the effects of three key parameters, NaFSI concentration, DMC/EMC ratio, and FEC content, on the performance of SIB using $NaNi_{1/3}Fe_{1/3}Mn_{1/3}O_2$ and hard carbon as the positive and negative electrodes. A total of 132 electrolyte formulations were prepared using automated liquid handling, and their electrochemical performance was evaluated using multichannel full-cell measurements. Data-driven analysis employing machine learning revealed that NaFSI concentration plays the most critical role in enabling highly reversible charge−discharge behavior. Long-term cycling tests and interfacial composition analyses were further conducted to clarify the influence of electrolyte components on stability. Detailed studies focusing on high-NaFSI, FEC-containing electrolytes showed that EMC-rich formulations outperformed DMC-rich counterparts, maintaining Coulombic efficiencies over 99.6% even after 300 cycles. X-ray photoelectron spectroscopy confirmed that these stable systems promote the formation of NaF-rich interphases on both electrodes. These findings provide valuable insights into electrolyte design strategies for durable and efficient SIBs and highlight the utility of high-throughput experimentation coupled with machine learning for electrolyte discovery.

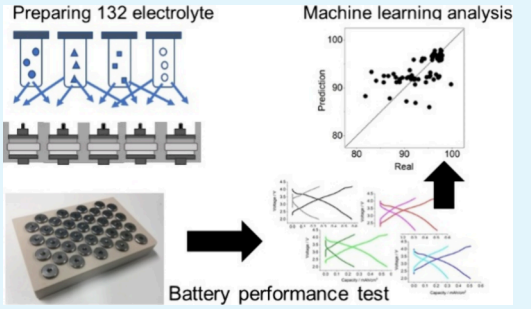

KEYWORDS: *high throughput experiment, sodium ion battery, multicomponent electrolyte, machine learning, solid-electrolyte interface*

INTRODUCTION

Sodium-ion batteries (SIBs) have garnered growing attention as a promising alternative to lithium-ion batteries (LiBs) for next-generation energy storage systems.[1,2] Owing to the natural abundance, low cost, and broad geographic distribution of sodium resources, SIBs offer a more sustainable and economically viable solution, particularly for large-scale applications such as grid storage. Furthermore, SIBs share similar intercalation chemistry and cell design as LiBs, allowing for relatively straightforward adaptation of existing technologies. Despite these advantages, SIBs are still at an earlier stage of development, and several key challenges must be addressed before their widespread commercialization. One of the most critical challenges lies in achieving long-term cycling stability, which is essential for the reliable operation of SIBs over extended periods. Among various factors influencing battery performance, the electrolyte plays a central role. It not only mediates ion transport but also governs the formation and evolution of the solid electrolyte interphase (SEI) on the anode and the cathode electrolyte interphase (CEI) on the cathode.[3,4] These interphases critically impact capacity retention, Coulombic efficiency, and overall cell lifespan. Designing a high-performance electrolyte is a highly intricate task, as it requires careful tuning of multiple interrelated parameters, including solvent polarity, salt concentration, solvation structure, the electrochemical stability window, and interfacial compatibility.

In practical battery systems, mixed-solvent electrolyte formulations are commonly used to balance the ionic conductivity, thermal and electrochemical stability, and interfacial properties. However, the rational selection of solvent combinations for SIBs remains largely empirical. The vast compositional space and the nonlinear interplay between components make it difficult to predict optimal electrolyte formulations. As a result, electrolyte discovery has traditionally relied on trial-and-error approaches, which are time-consuming

Received: September 26, 2025
Revised: December 24, 2025
Accepted: December 29, 2025
Published: January 16, 2026

Downloaded via NATL INST FOR MATLS SCIENCE (NIMS) on February 12, 2026 at 22:54:48 (UTC).
See https://pubs.acs.org/sharingguidelines for options on how to legitimately share published articles.

ACS Publications
© 2026 The Authors. Published by American Chemical Society

https://doi.org/10.1021/acsaem.5c03028
ACS Appl. Energy Mater. 2026, 9, 1405−1411

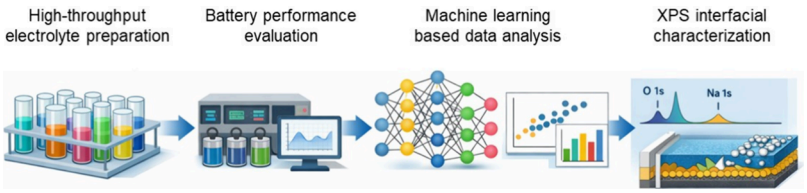

Figure 1. Schematic illustration of the overall workflow of the present study.

and resource-intensive. Recent advances in high-throughput experimentation and data-driven methodologies have demonstrated their effectiveness for transforming the landscape of materials discovery even in the field of rechargeable batteries.[5,6] In the context of solid-state materials, machine learning and computational screening have successfully guided the identification of promising candidates.[7,8] For liquid materials, such as electrolytes, high-throughput measurement techniques for fundamental physicochemical properties such as ionic conductivity and viscosity are now available.[9,10] However, translating these basic metrics into reliable predictions of electrochemical performance, particularly under realistic cycling conditions, remains a significant challenge. This is primarily due to the complexity of electrochemical reactions at interfaces and the lack of scalable methods for evaluating long-term battery performance in a high-throughput manner.

Based on this research background, we recently developed a modular high-throughput experimental platform that integrates automated liquid handling with parallel electrochemical testing.[11−13] Using LiB electrolyte systems as a model, we demonstrated the capability to evaluate hundreds of compositions in a systematic and reproducible manner.[14] This platform enables rapid screening of electrolyte candidates under conditions that closely mimic the real battery operation. In this study, we extend our high-throughput methodology to SIBs, aiming to accelerate the discovery of electrolyte formulations that promote long-term cycling stability. By systematically exploring a wide array of mixed-solvent systems, we seek to uncover correlations among electrolyte composition, interfacial behavior, and electrochemical performance. Our results provide valuable insights into the design principles governing electrolyte optimization for SIBs and demonstrate the power of high-throughput approaches in advancing next-generation battery technologies.

EXPERIMENTAL METHOD

Battery Performance Evaluation

The battery-grade chemicals, including NaFSI, EC, PC, DMC, EMC, and FEC, were purchased from Kishida Chemical Co., Ltd., with purities exceeding 99.9% for NaFSI and 99.5% for the solvent. The diameter of the interior of the cell was 9 mm. The glass fiber membrane (thickness: 100 μm, diameter: 6.4 mm) was employed as a separator. The hard carbon electrode and the $NaNi_{1/3}Fe_{1/3}Mn_{1/3}O_2$ electrode were used after drying in a vacuum.

For fabrication of MCE cells, electrode and separator sheets are punched into the desired size and inserted into MCE cells by using semiautomated punching equipment. One MCE cell module is prepared within 1 h and introduced into an Ar-filled Gl-box. Multicomponent electrolyte preparation and injection into the MCE cell were performed by a liquid handling dispenser (Gyger, CERTUS), which is installed inside of an Ar-filled Gl-box. The equipment realizes contactless dispensing of various kinds of liquid samples with different physical properties by utilizing eight individually controllable channels, using microvalve technology and air pressure control. The mother solution is supplied to the dispenser from 50 mL sized bottles to the dispensing channel through the tube. Calibration is performed for each mother solution by adjusting microvalve and air pressure control conditions, which enables the electrolyte injection with accuracy at the scale of 50 nL. Mother solutions were directly injected into each MCE cell with an appropriate solution volume ratio, resulting in the total volume of solution injected into each cell being controlled to be 40 μL. Notably, as the electrolyte injection is done by a dispensing system, the injected electrolyte is spontaneously mixed inside of the cell. An Au-coated SUS-based spring was introduced into each well, electrically connected, and controlling the confining pressure. Then, the top part of the MCE cell was tightly sealed by capping its top with bolts, thereby largely suppressing the volatilization of electrolyte.

Fabricated MCE cell modules were taken out from the Gl box and were subjected to a charge/discharge test using a battery cycler (Hokuto Denko, HJ1001SD8). During the battery performance test, the MCE cell was installed into a temperature-controlled chamber (ESPEC, LU-124). When the battery performance test was completed, the MCE cells were disassembled. The parts of bolts were opened, and electrodes, separators, and electric connection parts were taken out. Although the electrodes and separators were disposed of, the MCE cell itself and electric connection parts were washed and dried. For fabrication of coin-type cells, the same kinds of electrolyte and electrode materials that were utilized for MCE cells were also used.

XPS Analysis

The chemical composition of the electrode was analyzed by using an X-ray photoelectron spectrometer (VersaProbe II Scanning XPS Microprobe, ULVAC-PHY). The analytical samples of electrochemically measured electrodes were obtained by disassembling cells and washing and drying them in an Ar-filled glovebox. THF (tetrahydrofuran, wako) was utilized for washing electrodes. The samples were cut into pieces and directly subjected to analysis of XPS without exposure to the atmosphere by using a transfer vessel.

Machine Learning

The classification model was implemented using the Random Forest Classifier model available in scikit-learn.[15] We tuned the max depth hyperparameter using Grid Search CV with 10-fold cross-validation. Three different scoring metrics were tested: accuracy, recall, and F1-score. For the regression task, the Linear Regression model implemented in scikit-learn was employed.

RESULTS AND DISCUSSION

In the present study, we developed a systematic workflow to explore optimal electrolyte compositions for SIBs using a high-throughput experimental and data-driven approach. First, we evaluated the electrochemical performance of 132 electrolyte formulations comprising multiple organic solvents. Automated liquid handling dispensing and multichannel electrochemical measurement systems were employed to efficiently conduct this experiment (Figure 1). Subsequently, we applied machine learning techniques to the acquired data set in order to identify key parameters that contribute to achieving superior battery performance. After that, X-ray photoelectron spectroscopy (XPS) analysis of the electrode/electrolyte interface is performed for selected samples to further deepen our understanding of the reaction inside of the battery.

https://doi.org/10.1021/acsaem.5c03028
ACS Appl. Energy Mater. 2026, 9, 1405−1411

The battery performance evaluation was conducted using multichannel electrochemical cells (Figure S1), using Na-$Ni_{1/3}Fe_{1/3}Mn_{1/3}O_2$ and hard carbon as the positive and negative electrodes. The details of the design of multichannel electrochemical cells are described in our previous report.[14] A representative voltage profile is shown in Figure 2a. In this

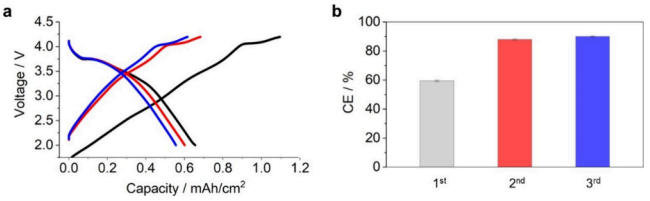

Figure 2. (a) Voltage profile of the sodium-ion battery cell operated at a current density of 0.2 mA/cm^2. (b) CE values in the first and third cycles, measured across three replicates (n = 3).

experiment, we use 1 M $NaPF_6$ in EC/EMC (50:50 vol %) as an electrolyte, and the measurement was performed under a current density of 0.2 mA cm^2 for three cycles. During the initial charging process, there can be a gradual increase of voltage and reached a cutoff voltage of 4.2 V. In the discharging process, the cell exhibited a stable profile, exhibiting a capacity of 0.78 mAh/cm^2. Figure 2b presents the value of Coulombic efficiency (CE) during the first to third cycles measured across three replicates (n = 3), with average values of 59.5, 88.0, and 90.0%, and standard deviations of 0.5, 0.4, and 0.3%, respectively. These results revealed the high reproducibility of the battery performance evaluation in the setup utilized in the present study.

In the present study, we focused on the multisolvent-based electrolyte system composed of ethylene carbonate (EC), propylene carbonate (PC), dimethyl carbonate (DMC), ethyl methyl carbonate (EMC), and fluoroethylene carbonate (FEC). NaFSI was selected as the sodium salt because of its high solubility in a wide range of solvents. By changing the amount of NaFSI and the ratio of each solvent, the various kinds of electrolyte with different compositions can be prepared. Electrolyte compositions were described based on molar ratios, based on our previous study.[14] In multicomponent electrolytes, using mol/L introduces problems because the total solution volume changes when solvents mix and large amounts of Li salt dissolve, making the final volume unpredictable and requiring measurement after preparation. Therefore, expressing all electrolyte components in terms of molar ratios offers a more precise and consistent method for describing the electrolyte composition.

While the roles of cyclic carbonates like EC and PC in battery performance and SEI formation are well investigated,[16,17] the effects of linear carbonates have been less explored. Yet, practical electrolytes often contain mixtures of linear carbonates such as DMC and EMC to optimize ion transport and interfacial stability. Therefore, this study specifically investigates the impact of the DMC/EMC ratio, with the cyclic carbonate content kept constant. Based on these considerations, we defined the electrolyte design space using three key compositional parameters: y (inverse value of NaFSI concentration), b (mol ratio of DMC in linear carbonate), and d (FEC concentration), which are defined as follows.

$$y = \frac{\mathrm{EC} + \mathrm{PC} + \mathrm{DMC} + \mathrm{EMC}}{\mathrm{NaFSI}}$$

$$b = \frac{\mathrm{DMC}}{\mathrm{DMC} + \mathrm{EMC}}$$

$$d = \frac{\mathrm{FEC}}{\mathrm{EC} + \mathrm{PC} + \mathrm{DMC} + \mathrm{EMC}}$$

Each parameter varied across the levels shown in Table S1. As a result, a total of 132 electrolytes are described by setting the specific values for these three parameters. These multisolvent electrolytes were experimentally prepared by using a liquid handling dispenser installed in an Ar-filled Gl-box (Figure 1b,c). In particular, 132 kinds of electrolytes were generated by combinatorial mixing of 9 kinds of mother solutions listed in Table S2.

To efficiently and accurately prepare electrolytes with diverse and complex compositions, we developed an integrated workflow that unifies the electrolyte formulation, mixing, and cell assembly within a single streamlined process. In this method, preassembled parallel electrochemical cells, in which each preloaded with a positive electrode, separator, and negative electrode, serve as standardized platforms for electrolyte introduction. A set of predefined mother solutions is dispensed directly into each cell in precise volumes by using an automated liquid handling system. After the electrolyte injection process is finished, the electric connection parts are installed in each cell. Then, the multichannel electrochemical cells are tightly sealed by capping their tops with bolts, which largely suppresses electrolyte volatilization. The multichannel electrochemical cells are then connected to a suitable multichannel battery tester via an electrochemical connection, which allows for the parallel measurement of battery performance for each cell (Figure 1d). In our experiments, the current density was set to be 0.2 mA/cm^2 for the first cycle and 0.5 mA/cm^2 for the next 10 cycles, with a cutoff voltage of 4.2 V/2.0 V condition. The first cycle was intentionally operated at a lower current density to serve as a conditioning step, allowing stable SEI formation before evaluating the intrinsic electrochemical behavior.

To apply machine learning techniques to analyze these data sets, we focused on the CE at the 11th cycle as the objective parameter. The 11th cycle was selected as a representative point because the initial cycles typically involve SEI formation and capacity stabilization, while later cycles exhibit smaller variations. Thus, the 11th cycle reflects the steady-state electrochemical behavior across all formulations. Although a variety of electrochemical parameters can be derived from the data set, we intentionally simplified the analysis by focusing on this single, widely recognized indicator of cell stability and reversibility to ensure clear and interpretable correlations. The summarized results are presented in Figure 3. We classified the battery performance into two categories based on the 11th CE values as follows:

Cyclable: 80% < 11th CE <100%

Noncyclable: 11th CE < 80 or ≥100%

By focusing on these data sets, a binary classification model using a random forest classifier was constructed to predict cyclability from electrolyte composition. Hyperparameters were initially tuned to maximize the accuracy score, resulting in a model accuracy of 0.9 via 10-fold cross-validation. Feature importance analysis revealed that the most influential parameters for achieving a stable CE were in order of y, d,

https://doi.org/10.1021/acsaem.5c03028
ACS Appl. Energy Mater. 2026, 9, 1405−1411

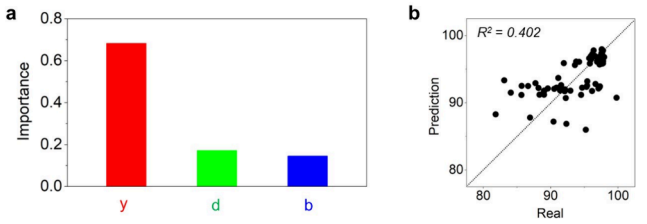

Figure 3. (a) Importance of parameters in the random forest classifier predicting cyclable/noncyclable. All data are used as training data, and the accuracy of the training data is 0.90. (b) Linear regression analysis with leave-one-out cross-validation.

and b (Figure 3a). Although the resulting precision was high (0.9375), the confusion matrix (Table 1) showed a large number of false negatives. To address this, the tuning objective was shifted to maximizing recall, which effectively reduced false negatives to 3. However, this trade-off led to an increased rate of false positives and a reduced precision of 0.808. This highlights the necessity of carefully considering the objective when performing hyperparameter tuning. Note that the confusion matrices for maximizing recall and maximizing the F1 score are summarized in Tables S3 and S4. In Figure 4, the histogram of samples showing higher CE is summarized, revealing that a low value of y (high concentration of NaFSI) is an effective guide for designing an electrolyte to achieve stable charge−discharge cycles.

Table 1. Confusion Matrix for Random Forest Classifier-Based Predictions of (Non) Cyclability Obtained Using the Leave-One-Out Cross-Validation

		prediction	
		cyclable	noncyclable
real	cyclable	75	8
	noncyclable	5	44

Furthermore, we attempted to construct predictive models for the CE value based on three explanatory variables: y, d, and b. Specifically, we focused on the subset of samples classified as Cyclable (11th CE values between 80 and 100%) and applied the linear regression technique (Figure 3b). The result revealed that the coefficient of determination (R^2) evaluated by the 10-fold cross-validation remained below 0.5, indicating a limited predictive performance. This result suggests that the CE values cannot be simply predicted from these three variables alone, indicating the complex and multifactorial nature of this system.

While our initial discussion just focused on the CE value of the 11th cycle, we extended our research scope for the long cycle stability. For this purpose, we exhibited 300th cycle tests on eight kinds of electrolyte compositions with two levels of NaFSI concentration (y = 0.6 or 1.0), in the presence and absence of FEC (d = 0 or 0.2), and the choice of solvent of EMC or DMC (b = 0 or 1). The 11th CE and the profile of CE during the cycling test and the representative voltage profile are summarized in Figure 5. For the EMC-based electrolyte, the cell without FEC (y = 6, d = 0, b = 0) showed a similar profile to that of the DMC-based electrolyte (y = 6, d = 0, b = 1). Initially, the cell exhibited the higher CE over 99%, and the value gradually decreased and reached approximately 98% at the 80th cycle. In sharp contrast, the cell with FEC-containing electrolytes (y = 6, d = 0.2, b = 0) exhibited CE above 99% over extended cycling. Notably, even at 300th cycles, the CE is higher than 99.6%. In the case of DMC-based electrolyte, the cell without FEC (y = 6, d = 0, b = 1) exhibited the gradual increase of CE and reached 99.2% at around the 20th cycle. However, with the progress of the cycle, the CE quickly decreased and reached below 98% by the 50th cycle. In contrast, the cell with FEC (y = 6, d = 0.2, b = 1) showed the higher CE over 99.4% even up to the 200th cycle, although the CE gradually decreased with the progress of the cycle and reached to 99% at the 300th cycle. The capacity retention of the series of SIB cells is summarized in Figure S2, which shows a trend consistent with the CE profiles. These results highlight that increasing the FEC concentration consistently enhances long-term CE retention regardless of the choice of main

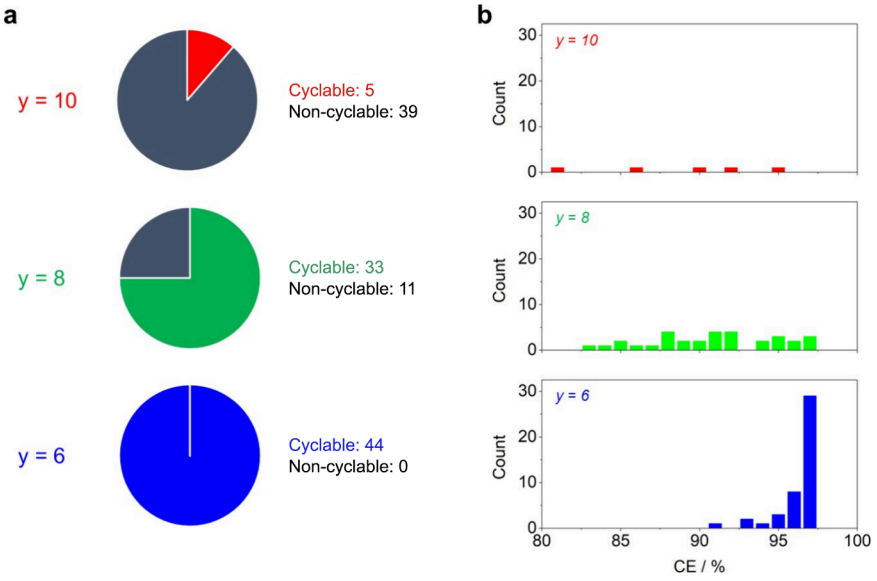

Figure 4. (a) Pie charts illustrating the relative proportions of cyclable and noncyclable outcomes for each y value. (b) Frequency table summarizing the distribution of CE values.

https://doi.org/10.1021/acsaem.5c03028
ACS Appl. Energy Mater. 2026, 9, 1405−1411

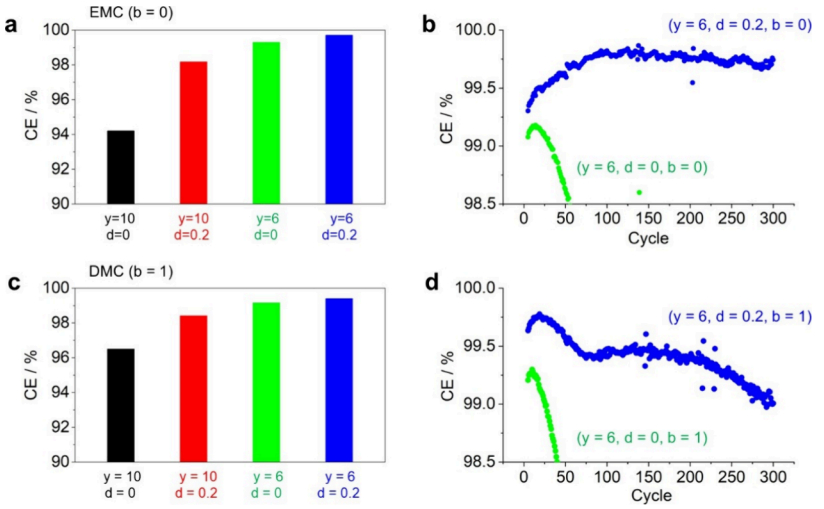

Figure 5. (a, c) Summary of 11th CE value for eight kinds of electrolyte. (b, d) Value of CE plotted against cycle number in repeated charge/discharge test.

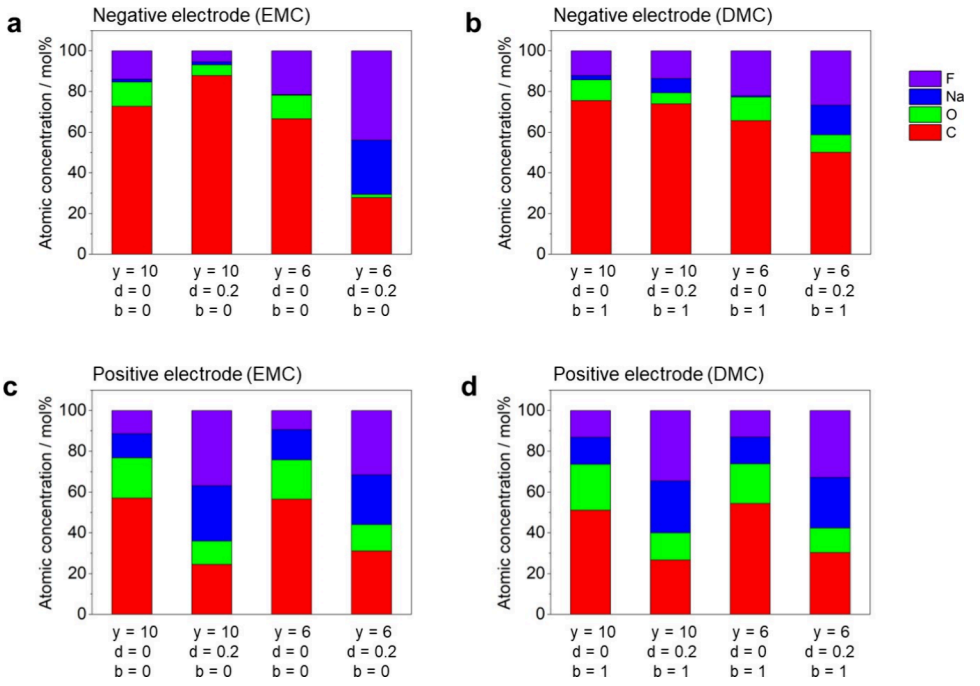

Figure 6. Chemical composition of (a, b) negative and (c, d) positive electrodes revealed by XPS analysis.

solvent (EMC or DMC). In addition, the EMC-based electrolyte formulation appears more promising for durability.

To elucidate the physicochemical origins of superior performance exhibited in FEC containing an EMC-based electrolyte, we analyzed the SEI formed on the hard carbon anode after the first charge using XPS. Figure 6 displays the elemental composition of the SEI formed in EMC-based electrolytes. High-concentration NaFSI with FEC yielded an SEI with ∼35% fluorine and negligible oxygen content, suggesting the formation of NaF-rich SEI layers. In contrast, electrolytes lacking FEC or with lower salt concentrations showed <3% fluorine and 10−20% oxygen, indicative of Na_2CO_3 or Na_2O-rich SEI layers.

Similar trends were observed in DMC-based systems, although the NaF content was generally lower than that of EMC-based counterparts. These findings suggest that EMC-based, high-NaFSI, FEC-containing electrolytes are most effective in forming NaF-rich SEI, which correlates with stable long-term CE. Actually, the several previous studies reported the positive effect of FEC and high NaFSI concentration on improving the performance of hard carbon electrodes in SIBs.[18−20] According to a previous computational study, DMC is more readily reduced than EMC.[21] Therefore, in DMC-rich electrolytes, DMC undergoes preferential decomposition during the early stages of SEI formation, yielding predominantly organic, solvent-derived SEI components. In contrast, in EMC-rich electrolytes, the higher reductive stability of EMC suppresses solvent decomposition. As a result, the reduction of FEC and, more importantly, the FSI anion proceeds more competitively than EMC reduction. This preferential anion-derived decomposition promotes the formation of NaF-rich SEI layers. While EIS measurements were not included in the

https://doi.org/10.1021/acsaem.5c03028
ACS Appl. Energy Mater. 2026, 9, 1405−1411

high-throughput platform, we have performed additional EIS tests for two representative electrolytes (high-NaFSI EMC-rich and DMC-rich). The results are summarized in Figure S3, confirming that EMC-rich formulations yield lower interfacial resistance, consistent with XPS findings. Taken together, these differences in the intrinsic reductive stability between DMC and EMC rationalize why EMC-rich electrolytes more effectively facilitate NaF-rich SEI formation.

The chemical composition of CEI was analyzed in a similar manner. In the absence of FEC (d = 0), CEI layers showed ∼15% fluorine and oxygen with no major differences between conditions. However, in FEC-containing systems (NaFSI: w/FEC and High-con NaFSI: w/FEC), the fluorine content increased to ∼25%, again suggesting NaF-rich CEI formation. These results confirm that the presence of FEC facilitates the generation of NaF-rich interphases on both electrodes, contributing to enhanced electrochemical stability. Taking together, these results suggest the following interfacial formation mechanisms governing SIB performance: (1) On the cathode side, the presence of FEC is sufficient to promote NaF-rich CEI formation, regardless of the solvent or salt concentration. (2) On the anode side, the formation of a NaF-rich SEI requires the synergistic combination of high NaFSI concentration, the presence of FEC, and EMC as the primary solvent. Considering the fact that the LiF-rich SEI and CEI have beneficial effects on the performance of LiBs,[22−26] the NaF-rich SEI/CEI is also considered to play a crucial role in suppressing side reactions, stabilizing electrode interfaces, and enabling high CE over long-term cycling in SIBs.

In optimizing electrolyte formulations, it is essential to consider not only SEI/CEI formation but also additional factors, such as ionic conductivity and material cost. Although ionic conductivity measurements were not included in the high-throughput platform, we conducted ionic conductivity tests for eight representative electrolyte compositions. The results show that DMC-rich electrolytes exhibit higher ionic conductivity than EMC-rich electrolytes, which can be attributed to the lower viscosity of DMC compared with EMC (Table S5). The introduction of FEC slightly decreases the ionic conductivity, consistent with the higher viscosity of FEC relative to DMC and EMC. Increasing the NaFSI concentration also leads to reduced conductivity. Consequently, the electrolyte composition that demonstrated the best cycling performance actually exhibited the lowest ionic conductivity among the tested formulations. This reflects a typical trade-off between long-term cycle stability and rate capability. Therefore, an EMC-rich electrolyte offers advantages not only in electrochemical performance but also in cost-effectiveness, providing an additional practical benefit.

In this study, our high-throughput experimental platform combined with data-driven analysis successfully enabled the rapid screening of a broad range of mixed-solvent electrolyte compositions for SIBs. We identified key compositional parameters that influence cycling stability, particularly the crucial role of high NaFSI concentrations and FEC additions in promoting stable Coulombic efficiency and long-term performance. The formation of NaF-rich SEI and CEI was revealed as a pivotal factor underpinning the enhanced electrochemical stability, especially in EMC-based electrolytes. These findings provide valuable design guidelines for future electrolyte optimization in SIBs, demonstrating the strength of integrating automated experimentation with machine learning for accelerating materials discovery.

CONCLUSIONS

In this study, we established a high-throughput experimental workflow for the systematic evaluation of electrolyte compositions in SIBs, enabling the rapid screening of 132 mixed-solvent formulations. By combining automated liquid handling with parallel electrochemical testing, we efficiently identified key compositional factors, namely, NaFSI concentration, FEC content, and the choice of cosolvent (DMC or EMC) that significantly influence Coulombic efficiency and long-term cycling stability. Machine learning analysis revealed that higher salt concentrations and the inclusion of FEC are critical for achieving a stable cycling performance. Further electrochemical and XPS analyses showed that the superior performance of FEC-containing EMC-based electrolytes is attributable to the formation of NaF-rich SEI and CEI layers, which enhance interfacial stability. Our findings provide practical guidelines for designing high-performance electrolyte systems for SIBs and demonstrate the power of data-driven, high-throughput approaches in accelerating electrolyte development for next-generation energy storage technologies.

ASSOCIATED CONTENT

Supporting Information

The Supporting Information is available free of charge at https://pubs.acs.org/doi/10.1021/acsaem.5c03028.

Photographic image of experimental setup; composition of mother solution; confusion matrix for random forest classifier-based predictions; profile of capacity retention; Nyquist plots; and ionic conductivity of electrolyte (PDF)

AUTHOR INFORMATION

Corresponding Authors

Ryo Tamura − *Center for Basic Research on Materials, National Institute for Materials Science, Tsukuba, Ibaraki 305-0044, Japan;* orcid.org/0000-0002-0349-358X; Email: TAMURA.Ryo@nims.go.jp

Shoichi Matsuda − *Center for Green Research on Energy and Environmental Materials, National Institute for Material Science, Tsukuba, Ibaraki 305-0044, Japan;* orcid.org/0000-0002-0640-3404; Email: MATSUDA.Shoichi@nims.go.jp

Authors

Manai Ono − *Center for Green Research on Energy and Environmental Materials, National Institute for Material Science, Tsukuba, Ibaraki 305-0044, Japan*

Misato Takahashi − *Center for Green Research on Energy and Environmental Materials, National Institute for Material Science, Tsukuba, Ibaraki 305-0044, Japan*

Complete contact information is available at: https://pubs.acs.org/10.1021/acsaem.5c03028

Notes

The authors declare no competing financial interest.

ACKNOWLEDGMENTS

The present work was supported by JST COI-NEXT (JPMJPF2016) and the Ministry of Education, Culture, Sports, Science, and Technology (MEXT) Program: Data Creation and Utilization Type Materials Research and Development

Project (JPMXP1121467561). The author also acknowledges the support from the National Institute for Materials Science (NIMS) Battery Research Platform.

REFERENCES

(1) Yabuuchi, N.; Kubota, K.; Dahbi, M.; Komaba, S. Research Development on Sodium-Ion Batteries. *Chem. Rev.* **2014**, *114* (23), 11636−11682.
(2) Zhang, F.; He, B.; Xin, Y.; Zhu, T.; Zhang, Y.; Wang, S.; Li, W.; Yang, Y.; Tian, H. Emerging Chemistry for Wide-Temperature Sodium-Ion Batteries. *Chem. Rev.* **2024**, *124* (8), 4778−4821.
(3) Pei, B.; Yu, H.; Zhang, L.; Fang, G.; Zhou, J.; Cao, X.; Liang, S. Hard Carbon for Sodium-Ion Batteries: From Fundamental Research to Practical Applications. *Adv. Mater.* **2025**, *37* (39), No. 2504574.
(4) Zhang, J.; Ma, S.; Zhang, J.; Zhang, J.; Wang, X.; Wen, L.; Tang, G.; Hu, M.; Wang, E.; Chen, W. Critical Review on Cathode Electrolyte Interphase towards Stabilization for Sodium-Ion Batteries. *Nano Energy* **2024**, *128*, No. 109814.
(5) Ng, M.-F.; Zhao, J.; Yan, Q.; Conduit, G. J.; Seh, Z. W. Predicting the State of Charge and Health of Batteries Using Data-Driven Machine Learning. *Nat. Mach. Intell.* **2020**, *2* (3), 161−170.
(6) Si, Q.; Matsuda, S.; Yamaji, Y.; Momma, T.; Tateyama, Y. Data-Driven Cycle Life Prediction of Lithium Metal-Based Rechargeable Battery Based on Discharge/Charge Capacity and Relaxation Features. *Adv. Sci.* **2024**, *11* (33), 2402608.
(7) Nishijima, M.; Ootani, T.; Kamimura, Y.; Sueki, T.; Esaki, S.; Murai, S.; Fujita, K.; Tanaka, K.; Ohira, K.; Koyama, Y.; Tanaka, I. Accelerated Discovery of Cathode Materials with Prolonged Cycle Life for Lithium-Ion Battery. *Nat. Commun.* **2014**, *5* (1), 4553.
(8) Jalem, R.; Kanamori, K.; Takeuchi, I.; Nakayama, M.; Yamasaki, H.; Saito, T. Bayesian-Driven First-Principles Calculations for Accelerating Exploration of Fast Ion Conductors for Rechargeable Battery Application. *Sci. Rep.* **2018**, *8* (1), 5845.
(9) Yan, P.; Fischer, M.; Martin, H.; Wölke, C.; Krishnamoorthy, A. N.; Cekic-Laskovic, I.; Diddens, D.; Winter, M.; Heuer, A. Non-Aqueous Battery Electrolytes: High-Throughput Experimentation and Machine Learning-Aided Optimization of Ionic Conductivity. *J. Mater. Chem. A* **2024**, *12* (30), 19123−19136.
(10) Rahmanian, F.; Vogler, M.; Wölke, C.; Yan, P.; Fuchs, S.; Winter, M.; Cekic-Laskovic, I.; Stein, H. S. Conductivity Experiments for Electrolyte Formulations and Their Automated Analysis. *Sci. Data* **2023**, *10* (1), 43.
(11) Matsuda, S.; Nishioka, K.; Nakanishi, S. High-Throughput Combinatorial Screening of Multi-Component Electrolyte Additives to Improve the Performance of Li Metal Secondary Batteries. *Sci. Rep.* **2019**, *9* (1), 6211.
(12) Matsuda, S.; Lambard, G.; Sodeyama, K. Data-Driven Automated Robotic Experiments Accelerate Discovery of Multi-Component Electrolyte for Rechargeable Li–O2 Batteries. *Cell Rep. Phys. Sci.* **2022**, *3* (4), No. 100832.
(13) Tamura, R.; Tsuda, K.; Matsuda, S. NIMS-OS: An Automation Software to Implement a Closed Loop between Artificial Intelligence and Robotic Experiments in Materials Science. *Sci. Technol. Adv. Mater. Methods* **2023**, *3* (1), 2232297.
(14) Matsuda, S.; Takahashi, M. Multichannel Electrochemical Cell and Liquid-Handling Dispenser for High-Throughput Combinatorial Screening of Multicomponent Electrolytes for Advanced Lithium-Ion Batteries. *Batter. Supercaps* **2025**, *8* (8), No. e202400777.
(15) Pedregosa, F.; Varoquaux, G.; Gramfort, A.; Michel, V.; Thirion, B.; Grisel, O.; Blondel, M.; Prettenhofer, P.; Weiss, R.; Dubourg, V.; Vanderplas, J.; Passos, A.; Cournapeau, D.; Brucher, M.; Perrot, M.; Duchesnay, E. Scikit-Learn: Machine Learning in Python. *J. Mach. Learn. Res.* **2011**, *12* (85), 2825−2830.
(16) Tasaki, K. Solvent Decompositions and Physical Properties of Decomposition Compounds in Li-Ion Battery Electrolytes Studied by DFT Calculations and Molecular Dynamics Simulations. *J. Phys. Chem. B* **2005**, *109* (7), 2920−2933.
(17) Hirsh, H. S.; Sayahpour, B.; Shen, A.; Li, W.; Lu, B.; Zhao, E.; Zhang, M.; Meng, Y. S. Role of Electrolyte in Stabilizing Hard Carbon as an Anode for Rechargeable Sodium-Ion Batteries with Long Cycle Life. *Energy Storage Mater.* **2021**, *42*, 78−87.
(18) Komaba, S.; Ishikawa, T.; Yabuuchi, N.; Murata, W.; Ito, A.; Ohsawa, Y. Fluorinated Ethylene Carbonate as Electrolyte Additive for Rechargeable Na Batteries. *ACS Appl. Mater. Interfaces* **2011**, *3* (11), 4165−4168.
(19) Fondard, J.; Irisarri, E.; Courrèges, C.; Palacin, M. R.; Ponrouch, A.; Dedryvère, R. SEI Composition on Hard Carbon in Na-Ion Batteries After Long Cycling: Influence of Salts (NaPF6, NaTFSI) and Additives (FEC, DMCF). *J. Electrochem. Soc.* **2020**, *167* (7), 70526.
(20) Takada, K.; Yamada, Y.; Watanabe, E.; Wang, J.; Sodeyama, K.; Tateyama, Y.; Hirata, K.; Kawase, T.; Yamada, A. Unusual Passivation Ability of Superconcentrated Electrolytes toward Hard Carbon Negative Electrodes in Sodium-Ion Batteries. *ACS Appl. Mater. Interfaces* **2017**, *9* (39), 33802−33809.
(21) Li, J.; Huang, S.; Yu, P.; Lv, Z.; Wu, K.; Li, J.; Ding, J.; Zhu, Q.; Xiao, X.; Nan, J.; Zuo, X. Unraveling the Underlying Mechanism of Good Electrochemical Performance of Hard Carbon in PC/EC−Based Electrolyte. *J. Colloid Interface Sci.* **2024**, *657*, 653−663.
(22) Chen, S.; Huang, L.; Wen, X.; Chen, Q.; Xia, Z.; Li, S.; Wang, H.; Xu, M.; Li, W. Formation Mechanism and Regulation of LiF in a Solid Electrolyte Interphase on Graphite Anodes in Carbonate Electrolytes. *J. Phys. Chem. C* **2023**, *127* (24), 11462−11471.
(23) Baek, M.; Kim, J.; Jin, J.; Choi, J. W. Photochemically Driven Solid Electrolyte Interphase for Extremely Fast-Charging Lithium-Ion Batteries. *Nat. Commun.* **2021**, *12* (1), 6807.
(24) Bai, P.; Ji, X.; Zhang, J.; Zhang, W.; Hou, S.; Su, H.; Li, M.; Deng, T.; Cao, L.; Liu, S.; He, X.; Xu, Y.; Wang, C. Formation of LiF-Rich Cathode-Electrolyte Interphase by Electrolyte Reduction. *Angew. Chemie Int. Ed.* **2022**, *61* (26), No. e202202731.
(25) Llanos, P. S.; Ahaliabadeh, Z.; Miikkulainen, V.; Lahtinen, J.; Yao, L.; Jiang, H.; Kankaanpää, T.; Kallio, T. M. High Voltage Cycling Stability of LiF-Coated NMC811 Electrode. *ACS Appl. Mater. Interfaces* **2024**, *16* (2), 2216−2230.
(26) Chen, L.; Nian, Q.; Ruan, D.; Fan, J.; Li, Y.; Chen, S.; Tan, L.; Luo, X.; Cui, Z.; Cheng, Y.; Li, C.; Ren, X. High-Safety and High-Efficiency Electrolyte Design for 4.6 V-Class Lithium-Ion Batteries with a Non-Solvating Flame-Retardant. *Chem. Sci.* **2023**, *14* (5), 1184−1193.

https://doi.org/10.1021/acsaem.5c03028
ACS Appl. Energy Mater. 2026, 9, 1405−1411